Performance Validation of In-House Developed Four-dimensional Dynamic Phantom

Rahul Kumar Chaudhary[1], Rajesh Kumar[1], S. D. Sharma[1,2], Soumen Bera[3], Vikram Mittal[3], Sudesh Deshpande[3]

[1]Radiological Physics and Advisory Division, Bhabha Atomic Research Centre, [2]Homi Bhabha National Institute, Anushakti Nagar, [3]P. D. Hinduja National Hospital and Medical Research Centre, Mumbai, Maharashtra, India

Abstract

Objective: The objective of this study was to validate the performance characteristics of in-house developed four-dimensional (4D) dynamic phantom (FDDP). **Materials and Methods:** There are three target inserts of 1.0, 1.5 and 2.0 cm diameter. The targets were driven in sinusoidal pattern in the longitudinal direction, using the combinations of amplitudes of 0.5, 1.0, and 1.5 cm with frequencies of 0.2 and 0.25 Hz. The amplitude and frequency of motion were measured manually, and by using Real-Time Position Management (RPM) system also. The static, free-breathing, and 4D computed tomography (CT) scans of the phantom were acquired with 1.0 mm slice thickness. The 4DCT scans were sorted into 0%–90% phase, and the maximum intensity projection (MIP) images were also generated. The static, free-breathing, and 4DCT data sets and MIP images were contoured to get V_{Static}, V_{FB}, V_{00}......V_{90}, and internal target volume ITV_{MIP}, respectively. The individual phase volumes were summed to obtain V_{4D}. The length of the target in the motion was measured using MIP image and compared with theoretical length (TL). The variation of 3D displacement vector of individual phase volume with respect to V_{00} with the phase of motion was studied at amplitude and frequency of 1.0 cm and 0.25 Hz, respectively. The degree of similarity between V_{FB} and V_{4D} and V_{FB} and ITV_{MIP} was also studied for all the target sizes at amplitude and frequency of 1.0 cm and 0.2 Hz and 1.0 cm and 0.25 Hz, respectively. **Results:** The amplitude and frequency of motion agreed within the limits of uncertainty with the manually and RPM measured values. The length of target in the motion matched within 1.0 mm with TL. The 3D displacement of individual phase volume showed no target size dependence, and the degree of similarity between V_{FB} and V_{4D} and V_{FB} and ITV_{MIP} decreases with increase in the displacement between the two volumes. **Conclusions:** The mechanical and imaging performances of FDDP were found within the acceptable limits. Therefore, this phantom can be used for quality assurance of 4D imaging process in radiotherapy.

Keywords: Four-dimensional computed tomography, four-dimensional radiotherapy, phase binning

INTRODUCTION

The respiration in the human body induces the movement in lung, liver, pancreas, and other thoracic and abdominal tumors.[1-5] If this breathing movement is not taken into account during the imaging, artifacts may occur. Distortion of the target volume occurs and this leads to incorrect information of position and volume.[6-18] The artifacts create difficulties in contouring the boundaries of the tumors, which may lead to failure in detecting the small moving volumes that are potentially cancerous. Addition of the treatment margins to account for the respiratory motion increases the field size and thus increases the volume of normal tissues exposed to high doses.

Several methods have been used in the past to take into account the tumor motion during the imaging or radiotherapy treatment planning.[19-22] Four-dimensional computed tomography (4DCT) is one of the methods of estimating the tumor motion. In the 4DCT, the moving tumor is imaged, and the synchronized motion of the surrogate marker is tracked by the tracking system. The software sorts out the images of the moving tumor into equally spaced phase bins, and the tumor images in each phase bin are contoured to obtain the tumor volume corresponding to that phase. The individual phase volumes are combined to obtain a volume

Address for correspondence: Mr. Rahul Kumar Chaudhary,
Radiological Physics and Advisory Division, CT and CRS Building,
Bhabha Atomic Research Centre, Anushakti Nagar, Mumbai - 400 094,
Maharashtra, India.
E-mail: rahulchaudhary1986@yahoo.co.in

Access this article online

Quick Response Code:

Website:
www.jmp.org.in

DOI:
10.4103/jmp.JMP_114_18

How to cite this article: Chaudhary RK, Kumar R, Sharma SD, Bera S, Mittal V, Deshpande S. Performance validation of in-house developed four-dimensional dynamic phantom. J Med Phys 2019;44:99-105.

that encompasses the motion of tumor during the entire respiratory cycle.

The use of 4DCT images for radiotherapy planning requires the knowledge of uncertainty in the tumor's position and volume. For this purpose, a dynamic phantom capable of simulating tumor motion is required. To meet this requirement, a dynamic phantom was designed and developed locally. The design of in-house developed phantom allows dose verification as well. In the past, many research groups[23-26] have developed the dynamic phantoms and different vendors have made it commercially available (Dynamic Breathing Phantom RS-1500 by Radiology Support Devices Inc., Long Beach, CA, USA; Quasar by Modus Medical Devices Inc., London, Canada; and Dynamic Thorax Phantom by CIRS, Norfolk, VA, USA). However, these commercially available dynamic phantoms have limited options and they are relatively costly. The dynamic phantom reported in this study provides wider range of amplitudes, frequencies, motion patterns along with the option of reproducing an arbitrary/patient-specific breathing pattern, and dose verification capabilities.

This study reports the results of the studies conducted to validate the mechanical and imaging performances of the in-house developed four-dimensional dynamic phantom (FDDP). To validate the mechanical performance of the in-house developed phantom, the accuracy and reproducibility of the motion were studied, and the imaging efficacy of this phantom was evaluated by measuring the length of the target in motion on the coronal section of the maximum intensity projection (MIP) image. The 3D displacements of the phase volumes with the phase of motion and the impact of motion on the target displacement have also been studied.

MATERIALS AND METHODS

Construction details of phantom
The in-house developed phantom is made up of polymethylmethacrylate (PMMA) and resembles the thorax section of the human body. The phantom contains cylindrical cavity where PMMA inserts of different types can be placed [Figure 1]. The first set of PMMA insert contains
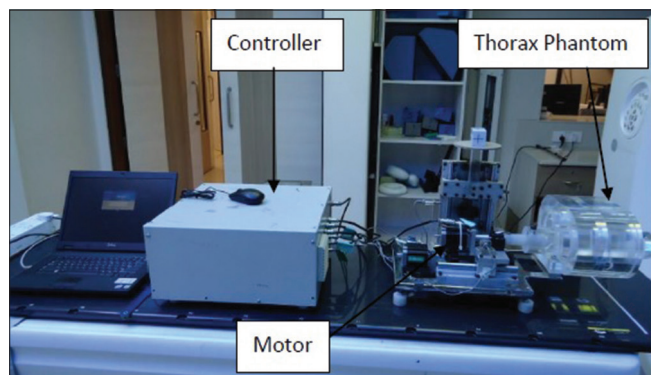
Figure 1: Photograph of the four-dimensional dynamic phantom showing its different components such as thorax phantom, motors, and controller unit

Delrin® spherical targets of diameters 1.0, 1.5, and 2.0 cm, whereas the second and third categories of PMMA inserts have provisions of accommodating CC13 small volume ionization chamber [Figures 2 and 3] and samples of radiochromic film, respectively, for the dosimetric purposes [Figure 4]. The cylindrical PMMA inserts are driven by two independent stepper motors: one for longitudinal motion and other for rotational motion. There is a platform on which the surrogate marker block is placed and the platform is driven in vertical direction by the third motor. The motions of all the motors of the phantom are synchronized and can also be varied independently.

The Real-Time Position Management (RPM) Respiratory Gating System (version 1.7.5, Varian Medical Systems, Palo Alto, CA), whose performance was thoroughly tested as per the standard protocols before putting into the clinical use, was used for tracking the motion of the surrogate marker.

Four-dimensional computed tomography scan
The phantom was set in sinusoidal motion with the following combinations of amplitude and frequency, respectively, (a) 0.5 cm, 0.2 Hz, (b) 1.0 cm, 0.2 Hz, (c) 1.5 cm, 0.2 Hz, (d) 0.5 cm, 0.25 Hz, (e) 1.0 cm, 0.25 Hz, and (f) 1.5 cm, 0.25 Hz, one by one for the spherical targets of diameter 1.0, 1.5, and 2.0 cm. In this experiment, the rotational motion of the phantom was turned off. The Discovery CT 590 RT (General Electric Company, Waukesha, WI) scanner was used for the 4DCT scans of the phantom. The static, free-breathing, and 4DCT scans of the phantom were acquired in the axial cine mode with 1.0 mm slice thickness; the number of images per rotation and the time of gantry rotation were set to 8 and 1.0 s, respectively. As per the standard protocol, the cine duration was kept 1.0 s more than the observed time period, and cine time between the images was set one-tenth of the observed time period.

Phase binning
The images of the moving target were acquired with the above-mentioned settings, and the 4DCT images were transferred to Advantage 4D Workstation (version 9.0, General Electric Company, Waukesha, WI), for phase sorting. The information regarding the moment of data acquisition is present in the DICOM image header which contains the timestamp. The reconstructed images and corresponding RPM data files were read by the software, and a phase was assigned to each image depending on the time of the data acquisition.[27] The acquired images were sorted into the different phase bins, ranging from 0% to 90% in the interval of 10%, and the MIP images were also generated. The static, free-breathing, and phase-binned 4DCT image data sets and MIP images were transferred to the Eclipse (version 13.6, Varian Medical Systems, Palo Alto, CA), treatment planning system (TPS) for contouring the target volumes.

Contouring of images
The static, free-breathing, 4DCT and MIP images were contoured manually by the same medical physicist on the TPS. To avoid intraobserver variation, the window level was set at

Figure 2: Polymethylmethacrylate inserts with Delrin® target of diameters 1.0, 1.5, and 2.0 cm from left to right (top row). Bottom row shows inserts of the same diameter as above, along with the cavity for placing different dosimeters

Figure 3: CC13 ionization chamber placed into the polymethylmethacrylate dosimetry insert

Figure 4: Cylindrical polymethylmethacrylate inserts for the target, ionization chamber, and radiochromic film samples, respectively (left to right)

700 HU with 1600 HU window width. The target volumes obtained by contouring the static, free-breathing, phase-binned 4DCT and MIP images were named as V_{Static}, V_{FB}, V_{00}...... V_{90}, and ITV_{MIP}, respectively. The individual phase volumes were combined to obtain V_{4D}. The combined volume encompasses all the positions of the target during the entire phases of the motion cycle.

Validation of mechanical and imaging performances of the phantom

To verify the mechanical performance, the phantom was set into the sinusoidal motion with the above-mentioned combinations of amplitudes and frequencies (Section B), one by one. The amplitude and frequency of motion of the surrogate marker were determined from the breathing curve files, generated during the tracking of the surrogate marker by the RPM system, and these values were compared with the respective values set on the FDDP. The parameters of sinusoidal motion (i.e., amplitude and frequency) were measured manually as well (using calibrated ruler and stopwatch).

The reproducibility of motion was verified by observing the motion pattern over the period of 3 months, for the phantom settings under the current study. The observed motion (obtained from RPM-generated breathing curve file) was fitted with equation:

$$y = y_0 + A \sin\left(\pi \frac{x - x_c}{w}\right), A > 0 \quad (1)$$

where y_0, A, x_c, and w are offset, amplitude of motion, phase shift, and the period of motion, respectively.

The imaging performance of the 4DCT system (software and phantom) was evaluated as per the Technical Quality Control Guidelines for Computed Tomography Simulators by the Canadian Partnership for Quality Radiotherapy;[28] the length (or amplitude) of the target in motion was measured on coronal MIP images for randomly selected combinations of target size, amplitude, and frequency of motion (a) 1.5 cm, 0.5 cm, 0.2 Hz, (b) 1.5 cm, 1.0 cm, 0.2 Hz, and (c) 2.0 cm, 1.5 cm, 0.25 Hz, respectively, and was compared with the theoretical length (TL). The TL is given by

$$TL = \text{Diameter of target } (2r) + 2A \quad (2)$$

where r is the radius of the target and A is the amplitude of the motion.

Variation of three-dimensional displacement of phase volume with phase of motion

The intrafractional displacements of the V_{10}, V_{20}......, V_{90} with respect to V_{00} in the anteroposterior (AP), left–right (LR), and superior–inferior (SI) directions were obtained from TPS, and 3D displacement was calculated by the following expression:[29]

$$3D \text{ displacement} = \sqrt{AP^2 + LR^2 + SI^2} \quad (3)$$

The 3D displacement of V_{10}, V_{20}......., V_{90} with respect to V_{00} was plotted against the phase of motion for the targets 1.0,

1.5, and 2.0 cm at amplitude and frequency of 1.0 cm and 0.25 Hz, respectively.

Impact of motion on the target displacement

The movement of the target results in the displacement of the center of mass (COM) of V_{4D} or ITV_{MIP} with respect to V_{FB}. The displacement of COM results in the variation of degree of overlap or similarity between the contoured target volumes. Dice similarity coefficient (DSC) was used to analyze the variation in the degree of overlap due to target displacement. DSC is an index having the value ranging from 0 to 1. The value 0 corresponds to completely nonoverlapping objects and the value 1 indicates that two objects are identical. The DSC is given by the following expression:

$$DSC = \frac{2\,|\,X \cap Y\,|}{|\,X\,| + |\,Y\,|} \tag{4}$$

where X and Y are the V_{FB} and V_{4D} or ITV_{MIP}, respectively.

RESULTS

Validation of mechanical and imaging performances of the phantom

The motions of the surrogate marker set at FDDP and measured by the RPM system for the combinations of amplitudes and frequencies of (a) 0.5 cm, 0.2 Hz and (b) 1.5 cm, 0.25 Hz are shown in Figure 5a and b, respectively. It is observed that there is an agreement between the amplitude and frequency of motion set at the FDDP and that measured by the RPM system. The results of the manually observed mechanical movements

are shown in Figure 6a and b for the set and observed values of the amplitudes and frequencies, respectively. Pearson's correlation coefficient value between the set and measured values was found to be 1, and the equation of fitted straight line was y = x. Thus, the manual tests also support the accuracy of mechanical movements of the phantom.

Figure 7 shows the observed motion pattern of the target, driven with amplitude and frequency of 1.5 cm and 0.2 Hz, respectively, over the period of 3 months. Table 1 shows the values and standard errors of fit parameters of the sinusoidal motion. The amplitude, frequency, and motion patterns of the phantom were reproducible over the period of observation. The motion was found reproducible for other combinations of amplitude and frequency as well. This validates the mechanical performance of the phantom.

The lengths of the targets measured on the coronal MIP image are shown in Figure 8a-c. It can be observed from these figures that the measured length of moving target agrees with TL within 1.0 mm variation. This validates the imaging performance of the in-house developed phantom.

### Variation of three-dimensional displacement of phase volume with phase of motion

The variation of 3D displacement of the phase volumes $(V_{10}, V_{20}....., V_{90}$ with respect to $V_{00})$ with the phase of motion is shown in Figure 9 for 1.0, 1.5, and 2.0 cm targets at the amplitude and frequency of 1.0 cm and 0.25 Hz, respectively. It is obvious that 3D displacement of the phase volumes with
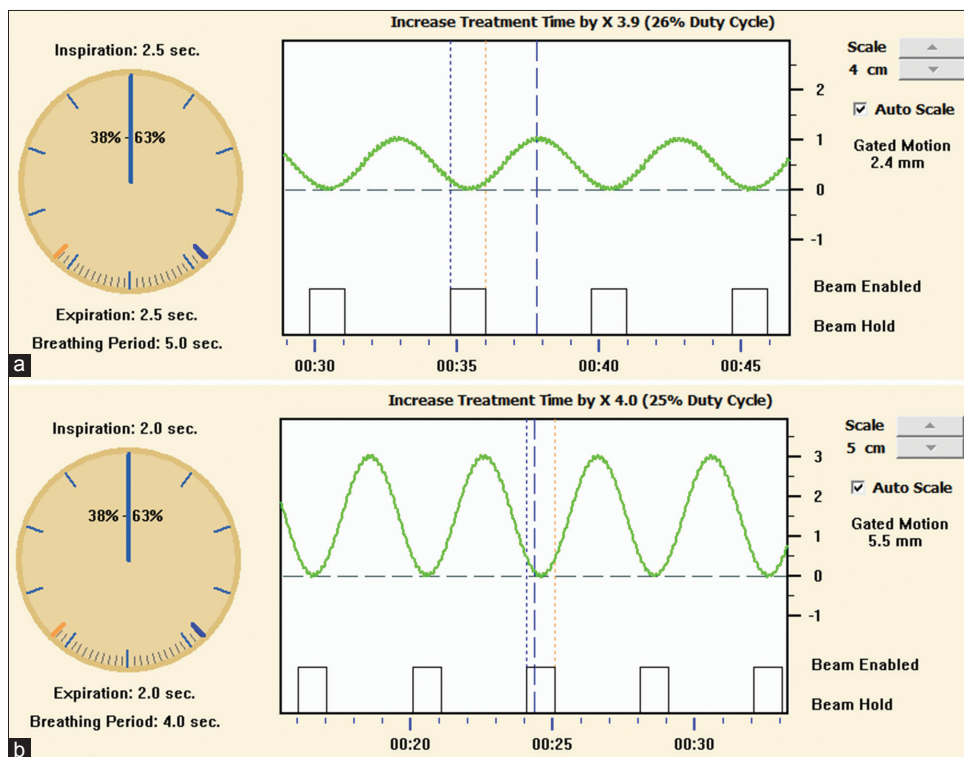
Figure 5: Motion of the surrogate marker, tracked by the Real-Time Position Management system for different combinations of amplitudes and frequencies (a) 0.5 cm, 0.2 Hz, and (b) 1.5 cm, 0.25 Hz, respectively
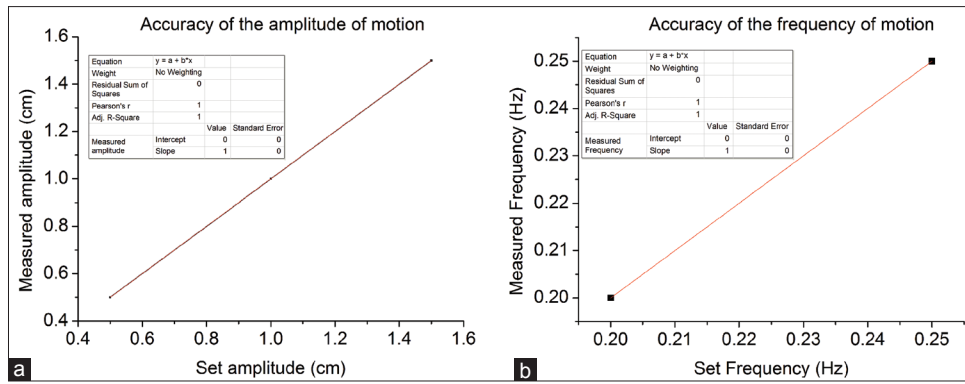
Figure 6: Graph showing the variation of set and manually measured values of the mechanical movements (a) amplitude and (b) frequency of the motion of the in-house developed phantom
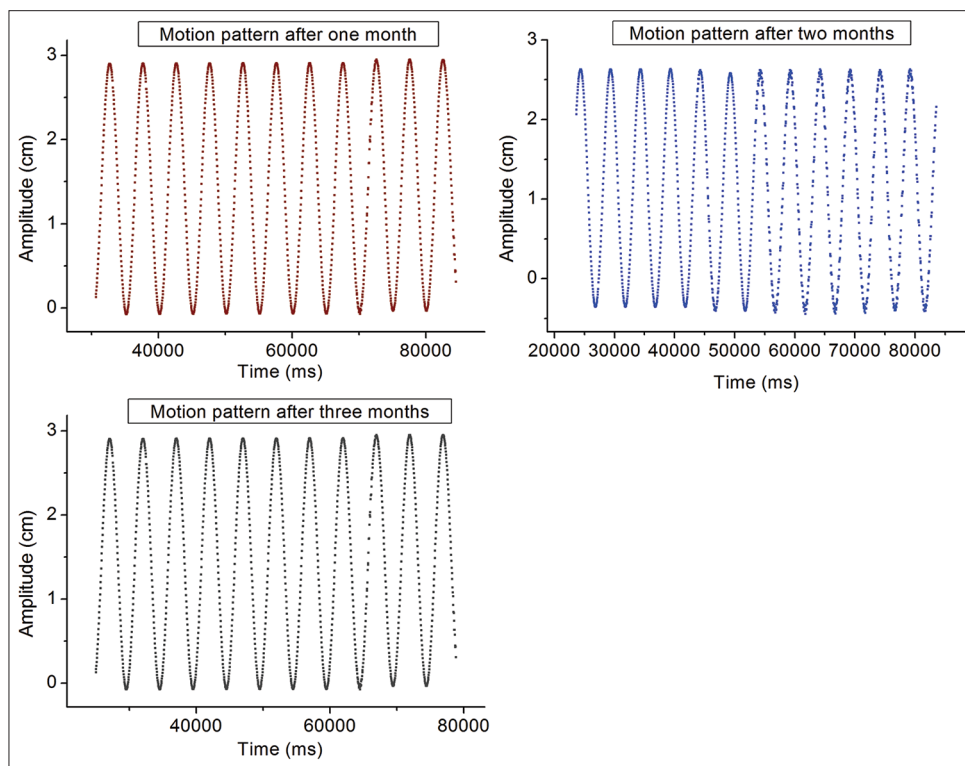
Figure 7: Observed motion pattern of the target, driven in sinusoidal pattern with amplitude and frequency of 1.5 cm and 0.2 Hz, respectively, after 1 month, 2 months, and 3 months

the phase of motion is independent of the size of the target used. Therefore, targets of all sizes have the same displacement for the given amplitude and frequency of motion.

Impact of motion on the target displacement

The DSC between V_{FB} and V_{4D} or V_{FB} and ITV_{MIP} along with the displacement of COM of V_{4D} or ITV_{MIP} with respect to V_{FB} are shown in Table 2 for 1.0, 1.5, and 2.0 cm targets for the following combinations of amplitude and frequency, respectively, (a) 1.0 cm, 0.2 Hz and (b) 1.0 cm, 0.25 Hz. From the data in Table 2, it can be observed that the DSC decreases as the displacement between the COM of V_{4D} or ITV_{MIP} with respect to V_{FB} increases. The DSC and displacement of COM

Table 1: Fit parameters of sinusoidal motion pattern observed after 1 month, 2 months, and 3 months

| Parameters	1 month		2 months		3 months	
	Value	SE	Value	SE	Value	SE
y_0	1.43	5.44×10^{-4}	1.11	7.69×10^{-4}	1.43	5.44×10^{-4}
x_c	1570.78	1.50	3175.82	1.79	898.08	1.38
w	2492.15	0.06	2492.09	0.08	2492.15	0.06
A	1.49	7.73×10^{-4}	1.49	1.09×10^{-3}	1.49	7.73×10^{-4}

SE: Standard error

values for V_{4D} and ITV_{MIP} are almost equal; Figure 10a-f shows the overlap between V_{FB}, V_{4D}, and ITV_{MIP} for 1.0, 1.5,

and 2.0 cm targets for the combinations of amplitudes and frequencies under the study.

DISCUSSION

The validation of mechanical performance of in-house developed FDDP was carried out, and the measured
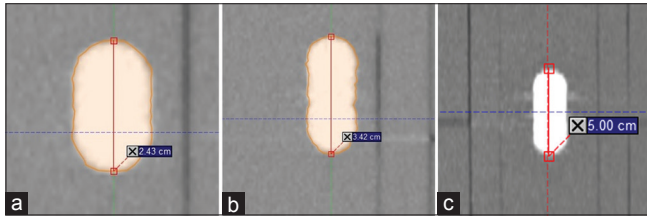
Figure 8: Length of the target, measured using coronal maximum intensity projection images for the combinations of target size, amplitude, and frequency of (a) 1.5 cm, 0.5 cm, 0.2 Hz, (b) 1.5 cm, 1.0 cm, 0.2 Hz, and (c) 2.0 cm, 1.5 cm, 0.25 Hz, respectively
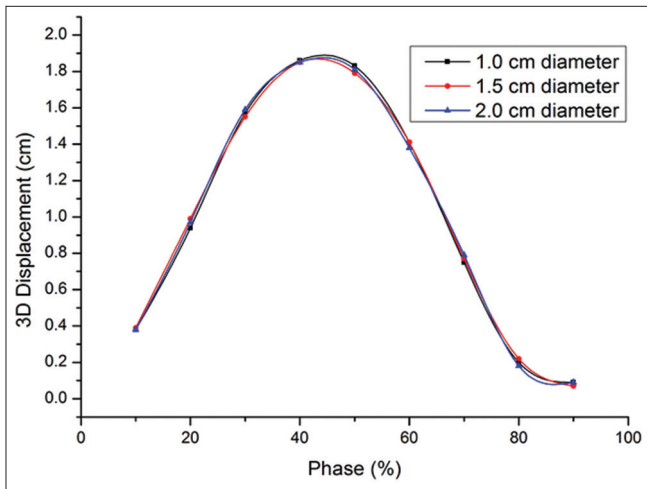
Figure 9: Variation of three-dimensional displacement with the phase of the motion for 1.0, 1.5, and 2.0 cm targets at the amplitude and frequency of 1.0 cm and 0.25 Hz, respectively
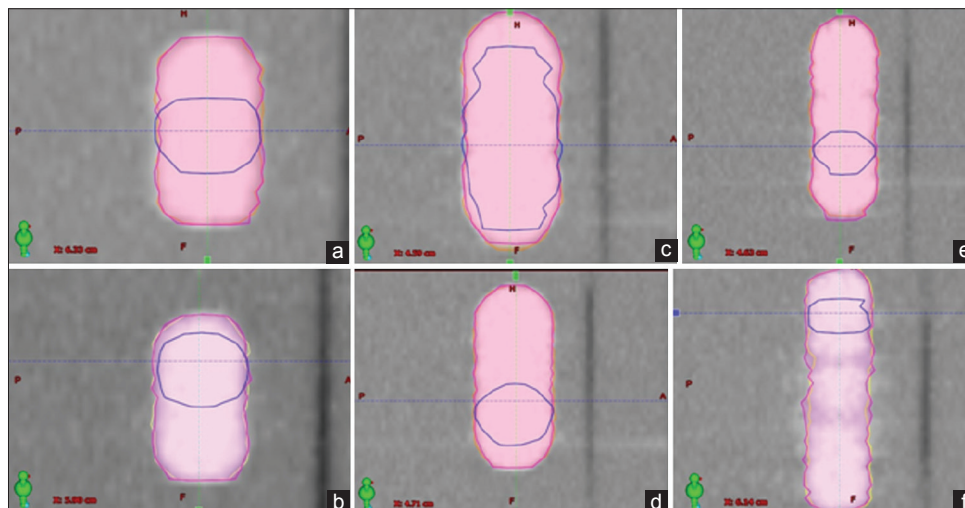
values of amplitude and frequency of motion agreed with the values set on the FDDP. The phantom's motion was monitored manually before using it for the imaging studies. The accuracy and reproducibility of the motion indicate the stability of the mechanical performance of the phantom. The agreement of the target length on the MIP image with TL validates the imaging accuracy of the phantom. Therefore, the in-house developed FDDP can be used for carrying out further imaging and clinical dosimetric studies. All the tests were carried out using ideal sinusoidal breathing pattern, whereas real breathing patterns are different.

The variation of 3D displacement vector of individual phase volume with respect to 0% phase with the phase of motion is independent of the target size for the given amplitude and frequency of motion. This result is an indication of the uniform velocity of the motion of the target, driven by the stepper motors of the developed phantom. Because of uniform velocity

Table 2: Dice similarity coefficient and displacement of center of mass of ITV_{MIP} and V_{4D} with respect to V_{FB} for 1.0, 1.5, and 2.0 cm targets at amplitude and frequency of 1.0 cm and 0.2 Hz and 1.0 cm and 0.25 Hz, respectively

Target diameter (cm)	Value	Amplitude (cm) and frequency (Hz)			
		1.0 and 0.2		1.0 and 0.25	
		ITV_{MIP}	V_{4D}	ITV_{MIP}	V_{4D}
1.0	DSC	0.78	0.79	0.38	0.38
	Displacement (cm)	0.19	0.18	0.66	0.68
1.5	DSC	0.20	0.21	0.29	0.31
	Displacement (cm)	0.15	0.15	0.07	0.07
2.0	DSC	0.30	0.29	0.34	0.34
	Displacement (cm)	0.52	0.52	0.34	0.33

DSC: Dice similarity coefficient, MIP: Maximum intensity projection, ITV: Internal Target Volume

Figure 10: The overlap between V_{FB} (blue contour), ITV_{MIP} (orange contour), and V_{4D} (magenta contour) for target sizes 1.0 cm, 1.5 cm, and 2.0 cm (left to right) at amplitude and frequency of 1.0 cm, 0.2 Hz (a, c, and e), and 1.0 cm, 0.25 Hz (b, d, and f), respectively

of the motion, the target is displaced by an equal amount in equal intervals of time. Here, the intervals of the cyclic motion are sorted out by the software into different phase bins.

The COM of the contoured volumes is displaced with the imparted motion. Due to the displacement of COM, the DSC between the volumes also varies; smaller COM displacement of V_{4D} or ITV_{MIP} with respect to V_{FB} results in greater overlap between the two volumes and hence results in higher DSC values as expected. The nearly equal values of the DSC for V_{4D} and ITV_{MIP} indicate large degree of overlap between the two volumes. This fact supports the past studies that ITV_{MIP} can be used as an alternate of V_{4D} for target delineation.[30]

Conclusions

The validation of mechanical and imaging performances and agreement with the past study gives the confidence that the FDDP has the potential to be used as a quality assurance tool for 4D imaging process in radiotherapy.

Conflicts of interest

There are no conflicts of interest.

References

1. Ohara K, Okumura T, Akisada M, Inada T, Mori T, Yokota H, *et al.* Irradiation synchronized with respiration gate. Int J Radiat Oncol Biol Phys 1989;17:853-7.
2. Ross CS, Hussey DH, Pennington EC, Stanford W, Doornbos JF. Analysis of movement of intrathoracic neoplasms using ultrafast computerized tomography. Int J Radiat Oncol Biol Phys 1990;18:671-7.
3. Kubo HD, Hill BC. Respiration gated radiotherapy treatment: A technical study. Phys Med Biol 1996;41:83-91.
4. Van de Steene J, Van den Heuvel F, Bel A, Verellen D, De Mey J, Noppen M, *et al.* Electronic portal imaging with on-line correction of setup error in thoracic irradiation: Clinical evaluation. Int J Radiat Oncol Biol Phys 1998;40:967-76.
5. Fröhlich H, Döhring W. A simple device for breath-level monitoring during CT. Radiology 1985;156:235.
6. Mayo JR, Müller NL, Henkelman RM. The double-fissure sign: A motion artifact on thin-section CT scans. Radiology 1987;165:580-1.
7. Ritchie CJ, Hsieh J, Gard MF, Godwin JD, Kim Y, Crawford CR. Predictive respiratory gating: A new method to reduce motion artifacts on CT scans. Radiology 1994;190:847-52.
8. Shepp LA, Hilal SK, Schulz RA. The tuning fork artifact in computerized tomography. Comput Graph Image Process 1979;10:246-55.
9. Tarver RD, Conces DJ Jr., Godwin JD. Motion artifacts on CT simulate bronchiectasis. AJR Am J Roentgenol 1988;151:1117-9.
10. Shimizu S, Shirato H, Ogura S, Akita-Dosaka H, Kitamura K, Nishioka T, *et al.* Detection of lung tumor movement in real-time tumor-tracking radiotherapy. Int J Radiat Oncol Biol Phys 2001;51:304-10.
11. Keall PJ, Kini VR, Vedam SS, Mohan R. Potential radiotherapy improvements with respiratory gating. Australas Phys Eng Sci Med 2002;25:1-6.
12. Ritchie CJ, Godwin JD, Crawford CR, Stanford W, Anno H, Kim Y. Minimum scan speeds for suppression of motion artifacts in CT. Radiology 1992;185:37-42.
13. Shimizu S, Shirato H, Kagei K, Nishioka T, Bo X, Dosaka-Akita H, *et al.* Impact of respiratory movement on the computed tomographic images of small lung tumors in three-dimensional (3D) radiotherapy. Int J Radiat Oncol Biol Phys 2000;46:1127-33.
14. Vedam SS, Keall PJ, Kini VR, Mostafavi H, Shukla HP, Mohan R, *et al.* Acquiring a four-dimensional computed tomography dataset using an external respiratory signal. Phys Med Biol 2003;48:45-62.
15. Ford EC, Mageras GS, Yorke E, Ling CC. Respiration-correlated spiral CT: A method of measuring respiratory-induced anatomic motion for radiation treatment planning. Med Phys 2003;30:88-97.
16. Van Herk M, Remeijer P, Rasch C, Lebesque JV. The probability of correct target dosage: Dose-population histograms for deriving treatment margins in radiotherapy. Int J Radiat Oncol Biol Phys 2000;47:1121-35.
17. Balter JM, Ten Haken RK, Lawrence TS, Lam KL, Robertson JM. Uncertainties in CT-based radiation therapy treatment planning associated with patient breathing. Int J Radiat Oncol Biol Phys 1996;36:167-74.
18. Chen GT, Kung JH, Beaudette KP. Artifacts in computed tomography scanning of moving objects. Semin Radiat Oncol 2004;14:19-26.
19. Cheung PC, Sixel KE, Tirona R, Ung YC. Reproducibility of lung tumor position and reduction of lung mass within the planning target volume using active breathing control (ABC). Int J Radiat Oncol Biol Phys 2003;57:1437-42.
20. Ford EC, Mageras GS, Yorke E, Rosenzweig KE, Wagman R, Ling CC. Evaluation of respiratory movement during gated radiotherapy using film and electronic portal imaging. Int J Radiat Oncol Biol Phys 2002;52:522-31.
21. Mah D, Hanley J, Rosenzweig KE, Yorke E, Braban L, Ling CC, *et al.* Technical aspects of the deep inspiration breath-hold technique in the treatment of thoracic cancer. Int J Radiat Oncol Biol Phys 2000;48:1175-85.
22. Negoro Y, Nagata Y, Aoki T, Mizowaki T, Araki N, Takayama K, *et al.* The effectiveness of an immobilization device in conformal radiotherapy for lung tumor: Reduction of respiratory tumor movement and evaluation of the daily setup accuracy. Int J Radiat Oncol Biol Phys 2001;50:889-98.
23. Nioutsikou E, Richard N Symonds-Tayler J, Bedford JL, Webb S. Quantifying the effect of respiratory motion on lung tumour dosimetry with the aid of a breathing phantom with deforming lungs. Phys Med Biol 2006;51:3359-74.
24. Court LE, Seco J, Lu XQ, Ebe K, Mayo C, Ionascu D, *et al.* Use of a realistic breathing lung phantom to evaluate dose delivery errors. Med Phys 2010;37:5850-7.
25. Serban M, Heath E, Stroian G, Collins DL, Seuntjens J. A deformable phantom for 4D radiotherapy verification: Design and image registration evaluation. Med Phys 2008;35:1094-102.
26. Szegedi M, Rassiah-Szegedi P, Fullerton G, Wang B, Salter B. A proto-type design of a real-tissue phantom for the validation of deformation algorithms and 4D dose calculations. Phys Med Biol 2010;55:3685-99.
27. Rietzel E, Pan T, Chen GT. Four-dimensional computed tomography: Image formation and clinical protocol. Med Phys 2005;32:874-89.
28. Canadian Partnership for Quality Radiotherapy. Technical Quality Control Guidelines for Computed Tomography Simulators. 2019 April 11. Available from: https://www.cpqr.ca/programs/technical-quality-control.
29. Li F, Li J, Zhang Y, Xu M, Shang D, Fan T, *et al.* Geometrical differences in gross target volumes between 3DCT and 4DCT imaging in radiotherapy for non-small-cell lung cancer. J Radiat Res 2013;54:950-6.
30. Underberg RW, Lagerwaard FJ, Slotman BJ, Cuijpers JP, Senan S. Use of maximum intensity projections (MIP) for target volume generation in 4DCT scans for lung cancer. Int J Radiat Oncol Biol Phys 2005;63:253-60.